Catalysis Today 153 (2010) 193–199

Contents lists available at ScienceDirect

Catalysis Today

journal homepage: www.elsevier.com/locate/cattod

Enhancement of photocatalytic activity over $NaBiO_3$/BiOCl composite prepared by an in situ formation strategy

Xiaofeng Chang[a,b,c], Gang Yu[a,b,*], Jun Huang[a,b], Zheng Li[a,b], Shufeng Zhu[a,b], Pingfeng Yu[a,b], Cheng Cheng[d], Shubo Deng[a,b], Guangbin Ji[c]

[a] POPs Research Center, Tsinghua University, Beijing 100084, China
[b] Department of Environmental Science and Engineering, Tsinghua University, Beijing 100084, China
[c] College of Materials Science and Technology, Nanjing University of Aeronautics and Astronautics, Nanjing 210016, China
[d] Department of Materials, Loughborough University, Loughborough, Leicestershire LE11 3TU, United Kingdom

ARTICLE INFO

Article history:
Available online 8 April 2010

Keywords:
$NaBiO_3$
BiOCl
Composite photocatalysts
Heterostructure

ABSTRACT

$NaBiO_3$/BiOCl composite photocatalysts with heterostructure have been prepared by a novel in situ formation approach, by using $NaBiO_3$ and hydrochloric acid aqueous solutions as the raw materials. Under visible light ($\lambda > 400$ nm) irradiation, the photocatalytic activity of Rhodamine B over $NaBiO_3$/BiOCl photocatalysts has been evaluated. The results demonstrate that the combination of $NaBiO_3$ and BiOCl has a higher photocatalytic activity compared with single $NaBiO_3$ or BiOCl photocatalyst, due to more effective photo-excited electron-hole separation by the heterojunction semiconductor structure and also higher absorption capacity of $NaBiO_3$.

1. Introduction

Photocatalysis technology, which enables the solar energy to purify water and air [1], is highly expected to be an ideal "green" technology for water/air treatment. Until now, semiconductor combination, which constructs a heterojunction interface between two types of semiconductors with matching energy band gaps, has been widely applied because it enhances the photogenerated charge carriers separation, thus achieving better efficiency for the decomposition of the organic compounds in wastewater. Previously, many heterostructured semiconductors, such as Cu_2O/TiO_2 [2,3], Bi_2O_3/TiO_2 [3], CdS/TiO_2 [4], Fe_2O_3/TiO_2 [5], $FeTiO_3/TiO_2$ [6], $MoS_2(WS_2)/TiO_2$ [7], $CuAlO_2/TiO_2$ [8], Si/TiO_2 [9], $Co_3O_4/BiVO_4$ [10], $Bi_2O_3/BaTiO_3$ [11], $WO_3/CuBi_2O_4$ [12], $CaFe_2O_4/PbBi_2Nb_2O_9$ [13] have been reported as photocatalysis systems.

$NaBiO_3$, first reported by Kako et al. [14], is a new efficient photocatalyst under visible light irradiation. The photocatalytic removal and transformation of polycyclic aromatic hydrocarbons (PAHs) and sodium pentachlorophenate (PCP-Na) over $NaBiO_3$ have also been systematically studied [15,16]. Our previous works [17,18] demonstrate that, in the presence of halogen hydride, $NaBiO_3$ can be corroded to Bi-based oxyhalides crystals which have received lots of interests due to their potential applications in decomposing organic compounds for environmental remediation [19–21], photo-electrochemical conversion [22] and splitting water into hydrogen and oxygen gases [23]. Herein, we develop a new strategy for the in situ preparation of $NaBiO_3$/BiOCl composite photocatalysts with heterojunction structure to enhance the photocatalytic activity.

2. Experimental

2.1. Materials and preparation

Ultrapure water from the Milli-Q system (Millipore, USA) was used in this experiment. All chemicals (purchased from Sinopharm Chemical Regent Co., Ltd.) were analytical grade and used as received without further purification. The preparation method for $NaBiO_3$/BiOCl composites is as follows. 3 g $NaBiO_3 \cdot 2H_2O$ powders were immersed into 20 mL of water and 40 mL of absolute ethanol while being stirred at room temperature. After $NaBiO_3$ were dispersed in the water–ethanol solution, for the synthesis of BiOCl and $NaBiO_3$/BiOCl composite photocatalysts with different $NaBiO_3$:BiOCl molar ratio of 7.1%, 14.1% and 25.3%, 18, 10, 8.5 and 7 mL of HCl aqueous solutions (7.2 wt%) was added, respectively. After stirring for 40 min, the resulted products were separated by centrifugation, washed by absolute ethanol, and dried at 80 °C for 6 h in air before further characterizations and photocatalytic activity evaluations. Scheme 1 gives the illustration of the in situ preparation of $NaBiO_3$/BiOCl composite photocatalysts.

* Corresponding author at: POPs Research Center, Tsinghua University, Beijing 100084, China. Tel.: +86 10 6278 7137; fax: +86 10 6279 4006.
E-mail address: yg-den@tsinghua.edu.cn (G. Yu).

0920-5861/$ – see front matter © 2010 Elsevier B.V. All rights reserved.
doi:10.1016/j.cattod.2010.02.069

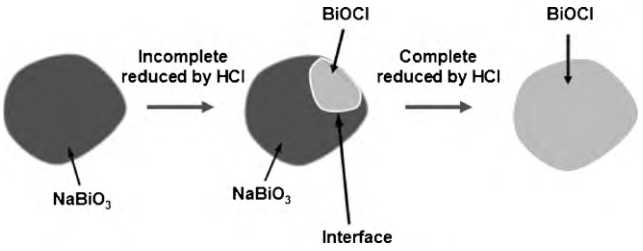

Scheme 1. Illustration of the in situ preparation of $NaBiO_3$/BiOCl composites.

2.2. Characterization and optical properties measurement

The crystal structures of the samples were analyzed by X-ray diffractionmeter (XRD, Bruker D8 ADVANCE). Scanning electron microscopy (SEM) and energy-dispersive X-ray spectroscopic (EDX) measurements were performed using a JSM 7401 field emission gun-scanning electron microscope. The N_2 adsorption–desorption analysis was measured on a NOVA 4000 (Quantachrome Corporation) instrument. Visible light diffuse reflectance spectroscopy (visible-light-DRS) was measured at room temperature on a Hitachi U-3010 spectrophotometer.

2.3. Batch sorption experiments and chemical analysis

For measuring the sorption isotherms, in dark condition, 0.08 g of BiOCl and $NaBiO_3$/BiOCl composite photocatalysts were transferred to flasks (250 mL), containing 200 mL of Rhodamine B(Rh. B) aqueous solution with different initial concentrations. These flasks were then transferred into an incubator shaker and shaken (at 150 rpm) for 48 h at a temperature of $25 \pm 2\,^{\circ}C$ to reach the adsorption–desorption equilibrium. Once the equilibrium was reached, the solid photocatalysts were separated by centrifuging at a speed of 4000 rpm for 15 min and the equilibrium concentration of Rh.B was detected by an UV–vis spectrometer at a wavelength of 554 nm.

2.4. Photocatalytic activity

The photocatalysis experiments of the samples were carried out in an XPA-Photochemical Reactor (Xujiang Electromechanical Plant, Nanjing, China). A Xenon lamp (500 W) was used as the light source. To ensure that the irradiation of the light system takes place only within the visible-light wavelengths, 2 M $NaNO_2$ aqueous solution was used to remove the radiation below 400 nm [24]. The photocatalyst dosage in the experiment was 0.4 g/L (initial concentration of Rh.B solution is 7.5 ppm) and the reaction temperature was kept at $20 \pm 2\,^{\circ}C$ by a water cooler machine (Lab Tech Company, USA). The slurry of reaction mixture was taken out and centrifuged at the speed of 4000 rpm for 15 min before the concentration determination.

3. Results and discussion

3.1. Characterization

Fig. 1 gives the XRD patterns (a), EDX patterns (b) and visible-light-DRS (c) of the pure phase of BiOCl and $NaBiO_3$/BiOCl photocatalysts with different compositions. The XRD and EDX results demonstrated that the molar ratio of $NaBiO_3$ (JCPDS card no. 30-1161) and BiOCl (JCPDS card no. 82-0485) crystals in the $NaBiO_3$/BiOCl composite photocatalysts can be well controlled by inducing different amounts of hydrochloric acid aqueous solutions. $NaBiO_3$ is an indirect transition semiconductor with the bandgap of 2.3–2.6 eV [14–16], indicating its visible light adsorption property. However, BiOCl is a type of wide bandgap semiconductor, the band gap range of which is 3.2–3.4 eV, according to the previous reports [20,21]. Therefore, it could be found that the visible-light-absorption ability of $NaBiO_3$/BiOCl composite photocatalysts can be improved by increasing the molar ratio of $NaBiO_3$ to BiOCl because of the visible-light responsibility of $NaBiO_3$. According to Kako et al., the long tail from Fig. 1(c) up to 620 nm could be possibly ascribed to the existence of lattice defects in $NaBiO_3$ crystal [14].

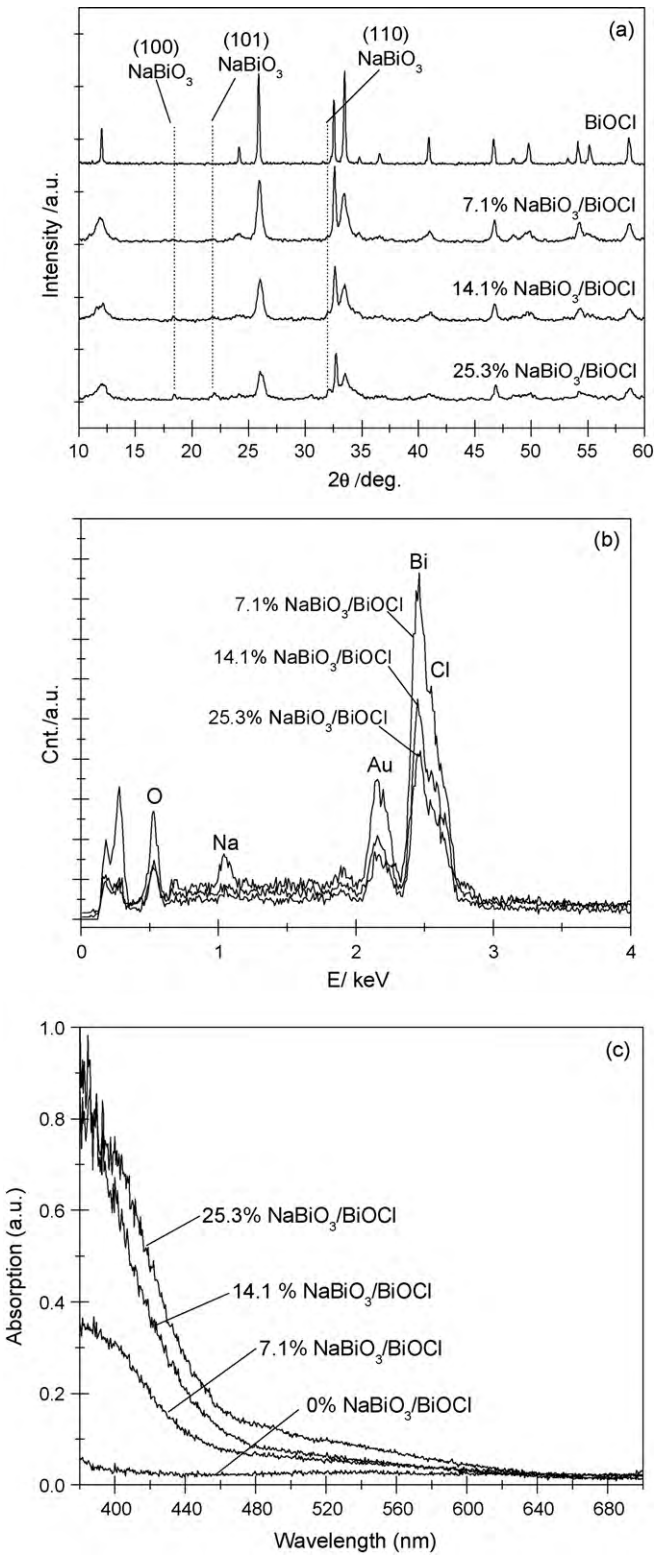

Fig. 1. XRD patterns (a), EDX patterns (b) and visible-light-DRS (c) of *x*% $NaBiO_3$/BiOCl composites.

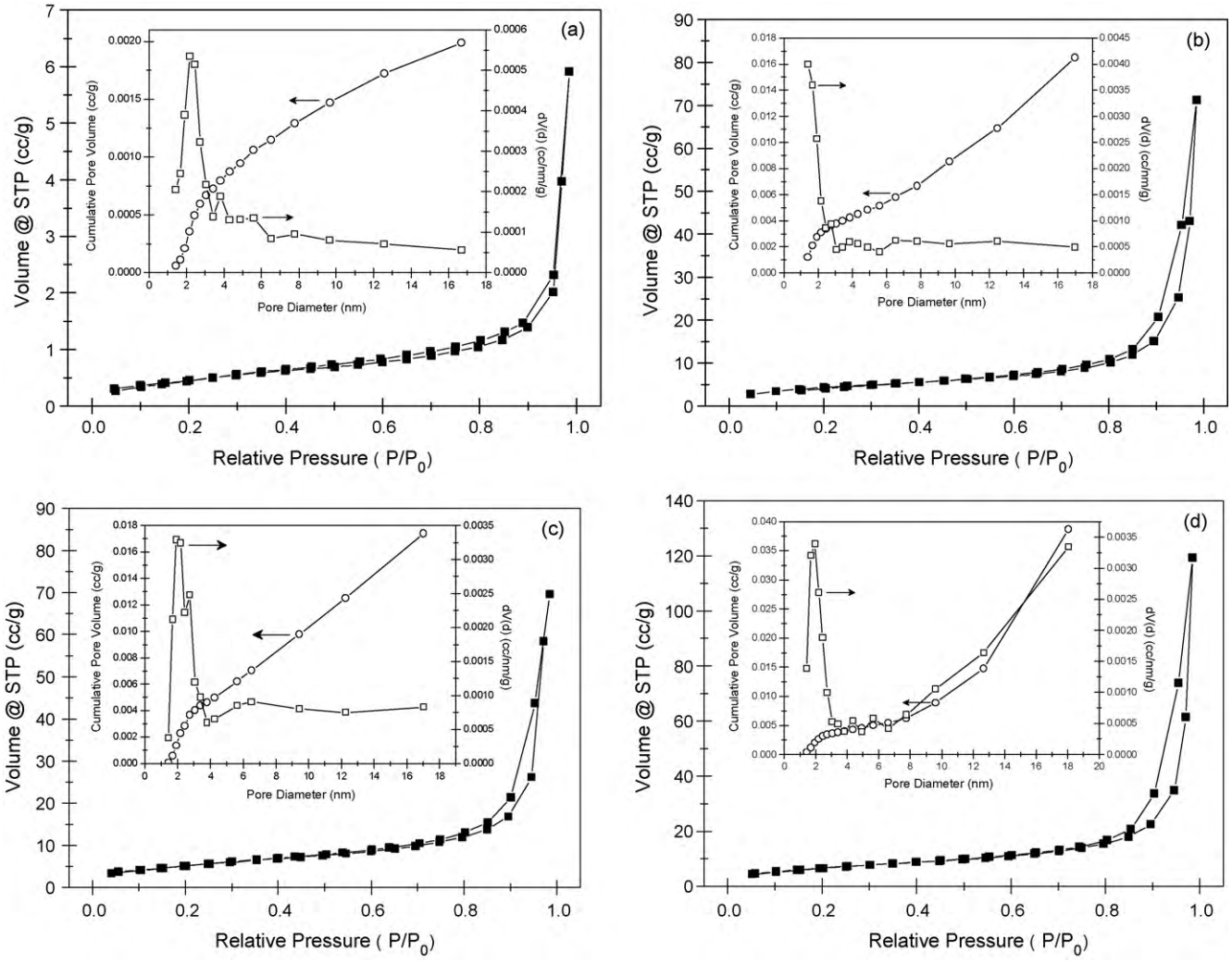

Fig. 2. N_2 adsorption–desorption isotherms and BJH pore size distributions from adsorption branch for the 0% $NaBiO_3$/BiOCl (a), 7.1% $NaBiO_3$/BiOCl (b), 14.1% $NaBiO_3$/BiOCl (c) and 25.3% $NaBiO_3$/BiOCl composites.

Fig. 2 shows the plots of nitrogen adsorption–desorption isotherms and BJH pore size distribution of BiOCl and the series $NaBiO_3$/BiOCl composite photocatalysts. It can be seen that both samples have sorption isotherms with a capillary condensation range starting at about $P/P_0 = 0.6$–0.7, extending to almost $P/P_0 = 1.0$. This suggests the textural porosity of the samples and it is deduced that the porous structure could be caused by the stacking of the sheet-like structure of the composite photocatalysts (Fig. 3).

3.2. Sorption isotherms

In order to evaluate the sorption capacity of the catalysts, and to understand the interactions between the catalysts and the molecules of the selected pollutant (namely, Rhodamine B), sorption isotherms of Rhodamine B molecules on BiOCl and the series $NaBiO_3$/BiOCl photocatalysts were investigated. The Langmuir and Freundlich equations, were adopted to describe the experimental data, which can be expressed respectively as,

$$q_e = \frac{q_m K_L C_e}{1 + K_L C_e} \quad (1)$$

$$q_e = K_F C_e^{1/n} \quad (2)$$

where q_e represents the equilibrium sorption amount (mg/g), C_e is the equilibrium concentration (mg/L) of Rhodamine B in solution, q_m is the maximum sorption capacity (mg/g), K_L is the sorption equilibrium constant (L/mg), K_F is a constant representing the sorption capacity ($mg^{1-1/n}\,L^{1/n}\,g^{-1}$), and n is a constant depicting the sorption intensity.

As given in Fig. 4 and Table 1, the sorption isotherms of Rhodamine B on the BiOCl and $NaBiO_3$/BiOCl photocatalysts can be better fitted by the Langmuir model than the Freundlich model. It should be noted that the Langmuir equation is obtained based on the assumption of monolayer coverage, and thus the better fitting results of the sorption of Rhodamine B on the $NaBiO_3$/BiOCl photocatalysts implying the possible occurred monolayer sorption. From the q_m value (obtained through the Langmuir model) and the specific surface area of $NaBiO_3$/BiOCl photocatalysts, the area covered by one Rh.B molecule (σ) can be calculated, as shown in Table 2. Such a small σ value suggests that condensed monomolecular layer of Rh.B covers over the $NaBiO_3$/BiOCl surface. On the other hand, the plateau regions in the sorption isotherms of Rh.B on such $NaBiO_3$/BiOCl composite photocatalysts could be the result of the condensed liquid being filled in these pores. Because of the microporous and mesoporous structure of the composites, the sorption saturation of the Rh.B molecule monolayer on the surface of the $NaBiO_3$/BiOCl composite photocatalysts could not be the actual reason of the plateau regions in the sorption isotherms, although the sorption isotherm results can be well modeled by Langmuir equation. Meanwhile, on the basis of the results obtained through the Langmuir model, it is surprising to find out that the sorption capac-

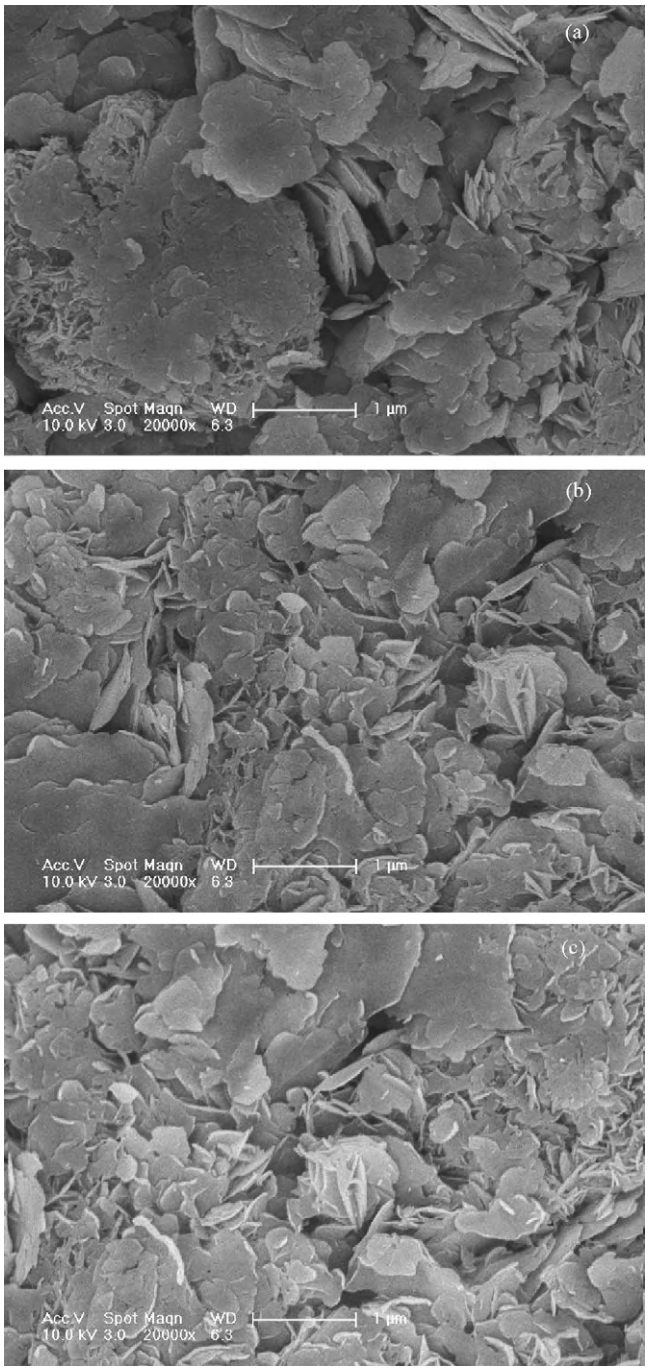

Fig. 3. SEM image of 7.1% (a), 14.1% (b) and 25.3% (c) $NaBiO_3$/BiOCl composites.

ity of Rhodamine B on the $NaBiO_3$/BiOCl photocatalysts was over 27–131 times as large as that on the pure BiOCl phase, possibly due to the larger sorption capacity of $NaBiO_3$ catalyst [14].

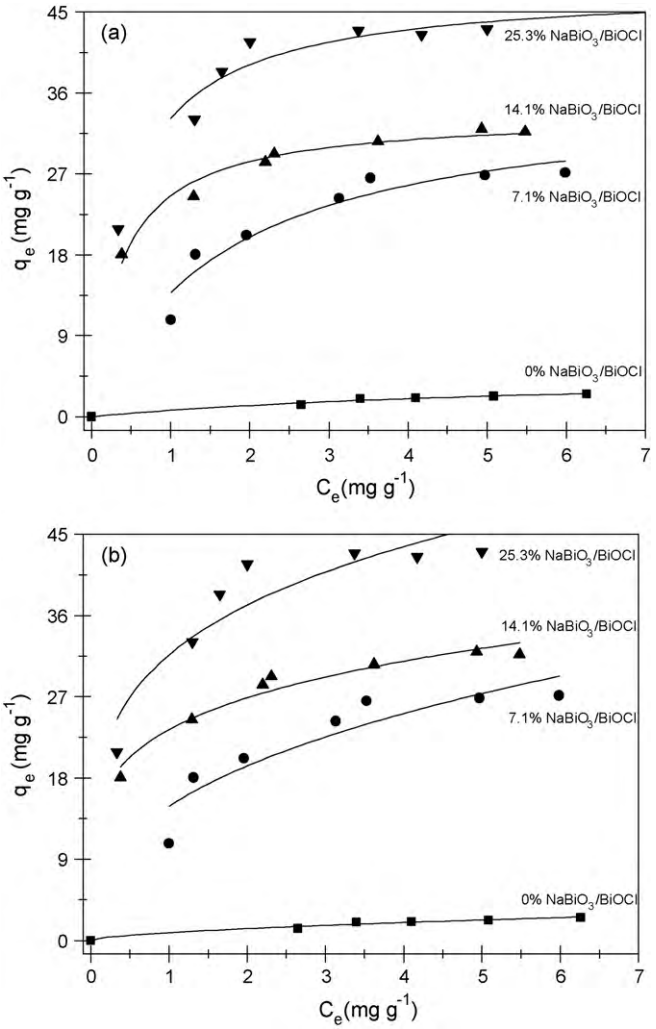

Fig. 4. Sorption isotherms of Rh.B on the BiOCl, 7.1% $NaBiO_3$/BiOCl, 14.1% $NaBiO_3$/BiOCl and 25.3% $NaBiO_3$/BiOCl composites at 25 °C and modeling using the Langmuir (a) and Freundlich equation (b).

Table 2
Some interface parameters of pure phase of BiOCl and $NaBiO_3$/BiOCl composites obtained from the N_2 adsorption–desorption isotherms, BJH pore size distribution results and Langmuir fitting.

x%	q_m (mmol g^{-1})	a (m^2 g^{-1})	σ (m^2)	D_a (nm)	V_p (cm^3 g^{-1})
0%	0.00172	1.748	0.16×10^{-23}	20.92	9.14E−03
7.1%	0.04663	15.802	0.49×10^{-23}	27.9	1.10E−01
14.1%	0.19029	19.091	1.66×10^{-23}	22.55	1.08E−01
25.3%	0.22628	24.508	1.53×10^{-23}	30.12	1.85E−01

Table 1
Calculated equilibrium constants using the Langmuir and Freundlich equations for Rh.B sorption on pure phase of BiOCl and series $NaBiO_3$/BiOCl photocatalysts.

x%	Langmuir			Freundlich		
	q_m (mg/g)	K_L (L/mg)	r^2	K_F ($mg^{1-1/n}$ $L^{1/n}$ g^{-1})	n^{-1}	r^2
0%	0.82622	0.16201	0.97871	0.86683	0.59709	0.97457
7.1%	22.33727	0.61821	0.91824	14.86787	0.37883	0.84794
14.1%	91.15282	2.71264	0.97042	23.35725	0.20274	0.95575
25.3%	108.39389	2.26955	0.96216	31.63199	0.23211	0.86552

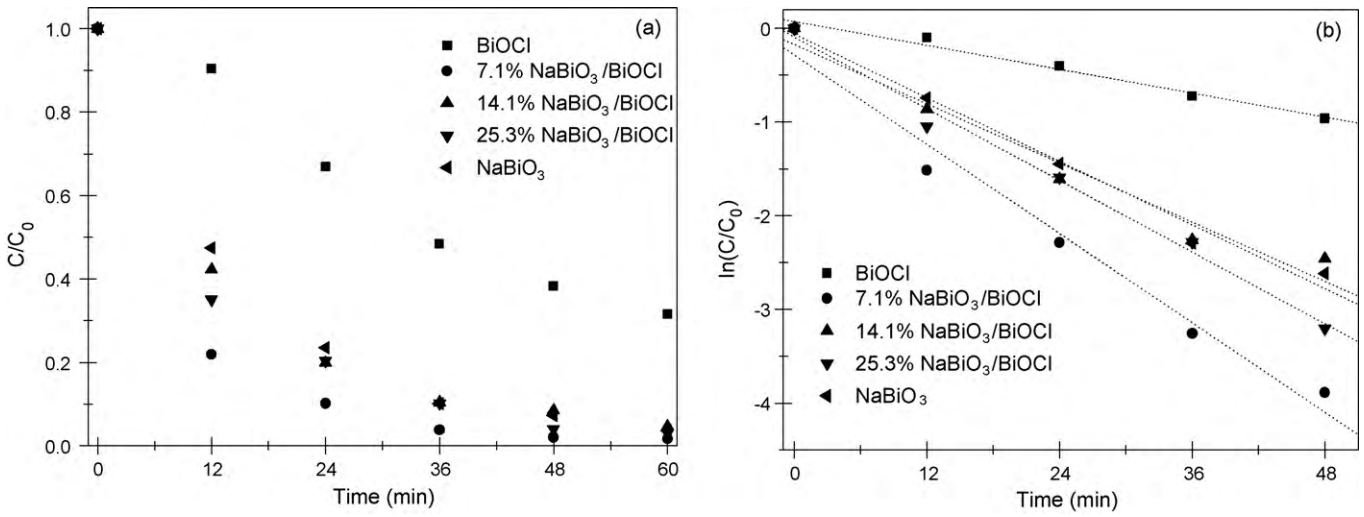

Fig. 5. Rh.B photocatalytically decomposed over pure phase of BiOCl, $NaBiO_3$ and $NaBiO_3$/BiOCl composites as a function of irradiation time and the pseudo first-order reaction kinetics.

3.3. Photocatalytic activity evaluation

Fig. 5 exhibits the photocatalytic activities of Rh.B dye on BiOCl and $NaBiO_3$/BiOCl photocatalysts. In comparison with the BiOCl, the $NaBiO_3$/BiOCl photocatalysts showed an improved photocatalytic activity under visible light irradiation. After 60 min of visible light irradiation, the removal efficiency of Rh.B by $NaBiO_3$/BiOCl composite photocatalysts and $NaBiO_3$ were over 90%. The results also proved that the Rh.B molecules can be decomposed over the wide bandgap BiOCl semiconductor (degradation efficiency was

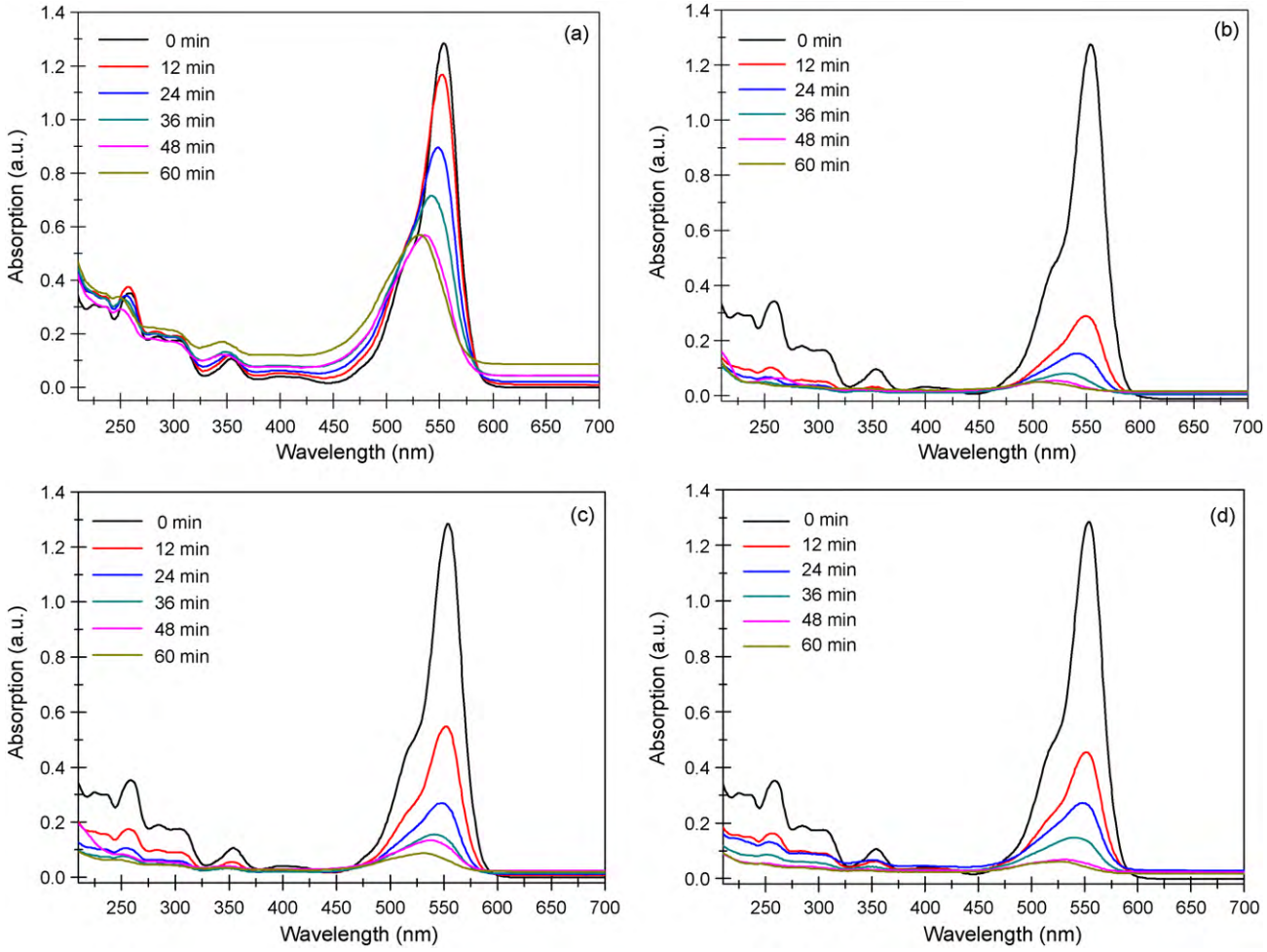

Fig. 6. UV–vis spectral changes of Rh.B aqueous solutions by using photocatalysts of BiOCl (a) 7.1% $NaBiO_3$/BiOCl (b), 14.1% $NaBiO_3$/BiOCl (c) and 25.3% $NaBiO_3$/BiOCl composites (d).

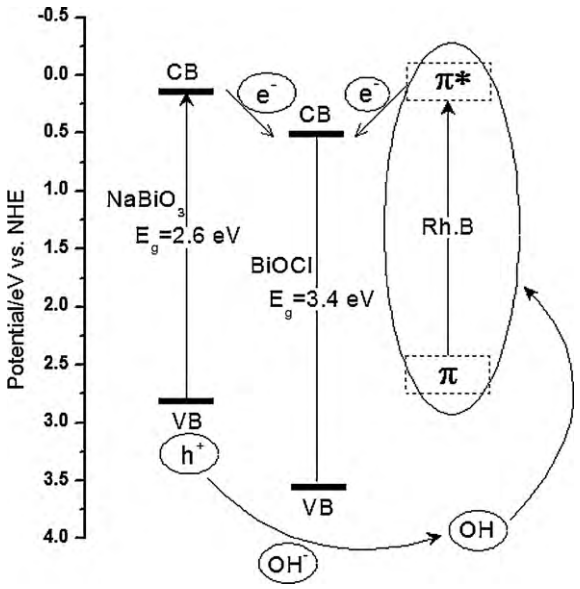

Fig. 7. Energetic diagram of $NaBiO_3$/BiOCl heterojunction.

~41%), possibly due to the effect of Rh.B dye sensitization on BiOCl semiconductor compounds [23].

The UV–vis spectra variations of Rh.B aqueous solutions (Fig. 6) show an obvious decrease in major absorption band at 554 nm. A concomitant wavelength shift of the band to shorter wavelengths (λ_{max} = 506 nm) could be observed apparently, demonstrating the intermediate products of de-ethylated Rh.B molecules were formed during the photocatalysis [25]. The result further demonstrates that the Rh.B molecules were effectively decomposed during the photocatalysis. From the discussion above, it is noted that the final decomposition efficiency (after 1 h) of BiOCl after combination with a small amount of $NaBiO_3$ could be as high as the pure $NaBiO_3$ photocatalyst. On the other hand, the pseudo first-order reaction kinetics of Rh.B decomposition under visible light irradiation was investigated and the K_r values were determined, the results of which are listed in Table 3. The result shows that photocatalytic reaction rates of series $NaBiO_3$/BiOCl composite photocatalysts were higher than that of pure $NaBiO_3$ and BiOCl photocatalyst, although the final removal efficiencies over $NaBiO_3$/BiOCl and $NaBiO_3$ photocatalysts were similar. This result is very important because it proves that the combination of $NaBiO_3$ and BiOCl can effectively improve the photocatalytic performance and result in a synergistic effect of "1 + 1 > 2".

The valence and conduction band edge (VB and CB) of BiOCl and $NaBiO_3$ semiconductors at the point of zero charge was calculated based on an atom's Mulliken electronegativity [26] and the predicted band edges were shown in Table 4. The predicted band edge potentials of BiOCl and $NaBiO_3$ suggest that the VB (or CB) potential of BiOCl are more positive (or negative) than those of $NaBiO_3$. It can be speculated that if under visible light irradiation, only $NaBiO_3$ semiconductor will be activated, the electrons generated to their conduction band are injected into the CB of inactivated BiOCl and the photogenerated holes from $NaBiO_3$ are not able to migrate to BiOCl, resulting in an effective electron-hole separation. Fig. 7 provides illustrations of interparticle electron transfer behavior under simulated solar light and visible light (λ > 400 nm) irradiation. Moreover, the superior photocatalytic activity of $NaBiO_3$/BiOCl composite photocatalysts upon visible light irradiation can be partially attributed to the high sorption capacity of $NaBiO_3$.

The XRD patterns of the series $NaBiO_3$/BiOCl blend photocatalysts after photocatalysis was also investigated and the results (given in Fig. 8) show that the XRD patterns were almost similar to

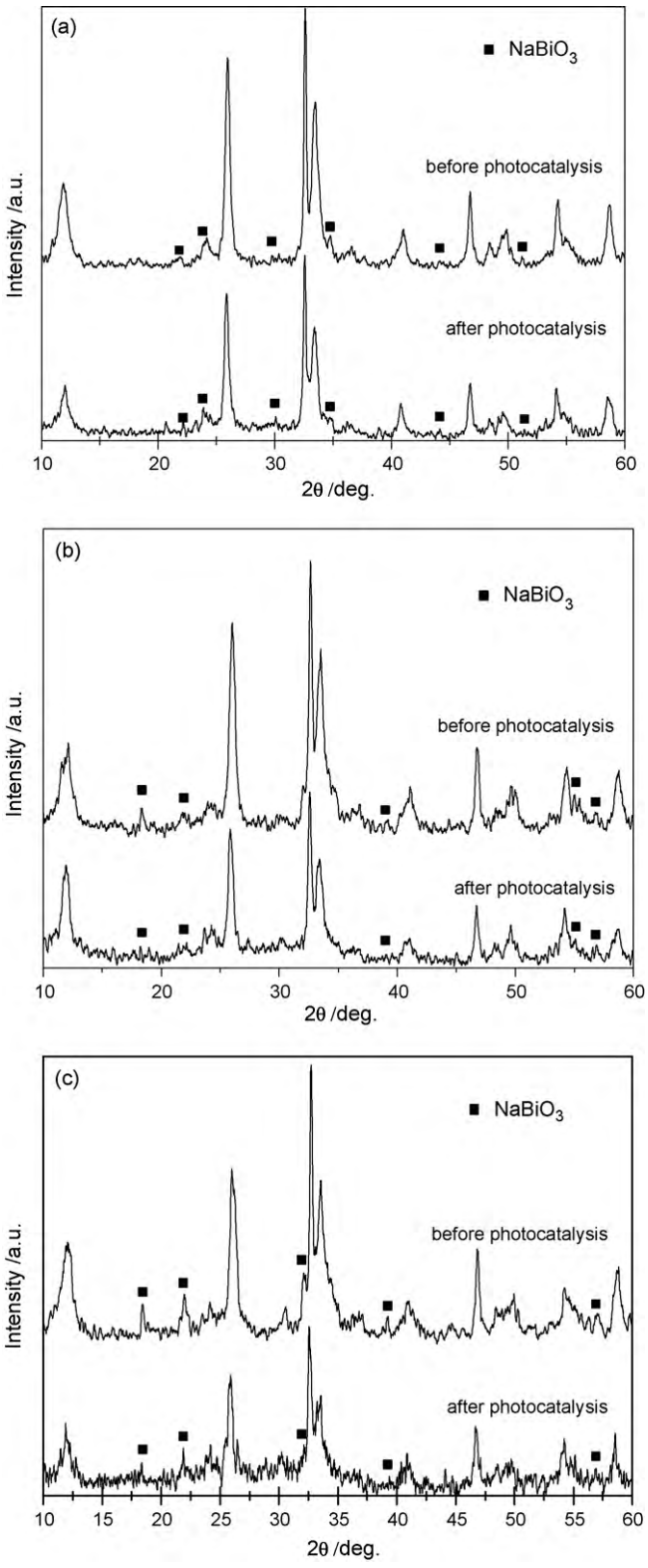

Fig. 8. XRD patterns of 7.1% $NaBiO_3$/BiOCl (a), 14.1% $NaBiO_3$/BiOCl (b) and 25.3% $NaBiO_3$/BiOCl composite photocatalysts (c) before and after photocatalysis.

those of the $NaBiO_3$/BiOCl photocatalysts before being used, suggesting the good chemical stability of the as-prepared $NaBiO_3$/BiOCl composite photocatalysts. As a type of heterogeneous photocatalysts, the $NaBiO_3$/BiOCl composite photocatalysts can be easily recycled by a simple filtration. Moreover, the sedimentation rate of series $NaBiO_3$/BiOCl composite photocatalysts in water was

Table 3
Photocatalytic kinetic results by using different catalysts.

	BiOCl	7.1% $NaBiO_3$/BiOCl	14.1% $NaBiO_3$/BiOCl	25.3% $NaBiO_3$/BiOCl	$NaBiO_3$
K_r (min^{-1})	0.02123	0.07937	0.05663	0.06373	0.05253
r^2	0.9784	0.97575	0.96144	0.98985	0.98514

Table 4
Absolute electronegativity, estimated band gap, calculated conduction band (CB) edge and valance band (VB) edge of BiOCl and $NaBiO_3$.

Catalyst	Absolute electronegativity (X/eV)	Estimated band gap (E_g/eV)	Calculated CB edge (E_{CB}/eV)	Calculated VB edge (E_{VB}/eV)
BiOCl	6.35901	3.19[a]/3.4[b][ref]	0.26401/0.15901	3.45401/3.55901
$NaBiO_3$	5.49579	2.3[a]/2.6[b][ref]	−0.15421/0.30421	2.14579/2.90421

[a] Estimated results.
[b] From references.

roughly calculated as ~0.18 cm s^{-1}, however, sedimentation rate of P25 which is a well known photocatalyst and has been widely studied for wastewater treatment, was only about ~0.004 cm s^{-1}. These results show good separability, which is an advantage for wastewater treatment.

4. Conclusions

$NaBiO_3$/BiOCl composite photocatalyst has been obtained by an in situ preparation approach, using $NaBiO_3$ and HCl aqueous solutions as the raw materials. An enhanced photocatalytic activity of $NaBiO_3$/BiOCl composite photocatalysts has been observed. Based on an atom's Mulliken electronegativity, it is found that effect of efficient charge separation on the $NaBiO_3$/BiOCl interface plays a key role for the catalytic enhancement. This study also showed the chemical stability and good separability of the as-prepared $NaBiO_3$/BiOCl composites.

Acknowledgements

This research was financially supported by National Science Fund for Distinguished Young Scholars of China (No. 50625823), National Key Project of Scientific and Technical Supporting Programs (No. 2007BAC03A09) and Program of Research on Key Technology of Environmental Pollution Control and Quality Improvement (No. 2007DFC90170).

References

[1] M.R. Hoffmann, S.T. Martin, W. Choi, D.W. Bahnemann, Environmental applications of semiconductor photocatalysis, Chem. Rev. 95 (1995) 69–96.
[2] Y. Zhang, L. Ma, J. Li, Y. Yu, In situ fenton reagent generated from TiO_2/Cu_2O composite film: a new way to utilize TiO_2 under visible light irradiation, Environ. Sci. Technol. 41 (2007) 6264–6269.
[3] Y. Bessekhouad, D. Robert, J.-V. Weber, Photocatalytic activity of Cu_2O/TiO_2, Bi_2O_3/TiO_2 and $ZnMn_2O_4$/TiO_2 heterojunctions, Catal. Today 101 (2005) 315–321.
[4] S. Banerjee, S.K. Mohapatra, P.P. Da, M. Misra, Synthesis of coupled semiconductor by filling 1D TiO_2 nanotubes with CdS, Chem. Mater. 20 (2008) 6784–6791.
[5] A.I. Kontos, V. Likodimos, T. Stergiopoulos, D.S. Tsoukleris, P. Falaras, Self-organized anodic TiO_2 nanotube arrays functionalized by iron oxide nanoparticles, Chem. Mater. 21 (2009) 662–672.
[6] B. Gao, Y.J. Kim, A.K. Chakraborty, W.I. Lee, Efficient decomposition of organic compounds with $FeTiO_3$/TiO_2 heterojunction under visible light irradiation, Appl. Catal. B: Environ. 83 (2008) 202–207.
[7] W. Ho, J.C. Yu, J. Lin, J. Yu, P. Li, Preparation and photocatalytic behavior of MoS_2 and WS_2 nanocluster sensitized TiO_2, Langmuir 20 (2004) 5865–5869.
[8] R. Brahimi, Y. Bessekhouad, A. Bouguelia, M. Trari, $CuAlO_2$/TiO_2 heterojunction applied to visible light H_2 production, J. Photochem. Photobiol. A: Chem. 186 (2007) 242–247.
[9] Y.J. Hwang, A. Boukai, P. Yang, High density n-Si/n-TiO_2 core/shell nanowire arrays with enhanced photoactivity, Nano Lett. 9 (2009) 410–415.
[10] M. Long, W. Cai, J. Cai, B. Zhou, X. Chai, Y. Wu, Efficient photocatalytic degradation of phenol over Co_3O_4/$BiVO_4$ composite under visible light irradiation, J. Phys. Chem. B 110 (2006) 20211–20216.
[11] X. Lin, J. Xing, W. Wang, Z. Shan, F. Xu, F. Huang, Photocatalytic activities of heterojunction semiconductors Bi_2O_3/$BaTiO_3$: a strategy for the design of efficient combined photocatalysts, J. Phys. Chem. C 111 (2007) 18288–18293.
[12] T. Arai, M. Yanagida, Y. Konishi, Y. Iwasaki, H. Sugihara, K. Sayama, Efficient complete oxidation of acetaldehyde into CO_2 over $CuBi_2O_4$/WO_3 composite photocatalyst under visible and UV light irradiation, J. Phys. Chem. C 111 (2007) 7574–7577.
[13] H.G. Kim, P.H. Borse, W. Choi, J.S. Lee, Photocatalytic nanodiodes for visible-light photocatalysis, Angew. Chem. Int. Ed. 44 (2005) 4585–4589.
[14] T. Kako, Z. Zou, M. Katagiri, J. Ye, Decomposition of organic compounds over $NaBiO_3$ under visible light irradiation, Chem. Mater. 19 (2007) 198–202.
[15] J. Kou, H. Zhang, Z. Li, S. Ouyang, J. Ye, Z. Zou, Photooxidation of polycyclic aromatic hydrocarbons over $NaBiO_3$ under visible light irradiation, Catal. Lett. 122 (2008) 131–137.
[16] X. Chang, G. Ji, Q. Sui, J. Huang, G. Yu, Rapid photocatalytic degradation of PCP-Na over $NaBiO_3$ driven by visible light irradiation, J. Hazard. Mater. 166 (2009) 728–733.
[17] X. Chang, J. Huang, C. Cheng, W. Sha, X. Li, G. Ji, S. Deng, G. Yu, Photocatalytic decomposition of 4-*t*-octylphenol over $NaBiO_3$ driven by visible light: catalytic kinetics and corrosion products characterization, J. Hazard. Mater. 173 (2010) 765–772.
[18] X. Chang, J. Huang, Q. Tan, M. Wang, G. Ji, S. Deng, G. Yu, Photocatalytic degradation of PCP-Na over BiOI nanosheets under simulated sunlight irradiation, Catal. Commun. 10 (2009) 1957–1961.
[19] S. Wu, C. Wang, Y. Cui, T. Wang, B. Huang, X. Zhang, X. Qin, P. Brault, Synthesis and photocatalytic properties of BiOCl nanowire arrays, Mater. Lett. 64 (2010) 115–118.
[20] K.L. Zhang, C.M. Liu, F.Q. Huang, C. Zheng, W.D. Wang, Study of the electronic structure and photocatalytic activity of the BiOCl photocatalyst, Appl. Catal. B: Environ. 68 (2006) 125–129.
[21] X. Zhang, Z. Ai, F. Jia, L. Zhang, Generalized one-pot synthesis, characterization, and photocatalytic activity of hierarchical BiOX (X = Cl, Br, I) nanoplate microspheres, J. Phys. Chem. C 112 (2008) 747–753.
[22] K. Zhao, X. Zhang, L. Zhang, The first BiOI-based solar cells, Electrochem. Commun. 11 (2009) 612–615.
[23] H. An, Y. Du, T. Wang, C. Wang, W. Hao, J. Zhang, Photocatalytic properties of BiOX (X = Cl, Br, and I), Rare Metals 27 (2008) 243–250.
[24] C. Lettmann, K. Hildenbrand, H. Kisch, Visible light photodegradation of 4-chlorophenol with a coke-containing titanium dioxide photocatalyst, Appl. Catal. B: Environ. 32 (2001) 215–227.
[25] H. Fu, C. Pan, W. Yao, Y. Zhu, Visible-light-induced degradation of Rhodamine B by nanosized Bi_2WO_6, J. Phys. Chem. B 109 (2005) 22432–22439.
[26] M.A. Butler, D.S. Ginley, Prediction of flatband potentials at semiconductor-electrolyte interfaces from atomic electronegativities, J. Electrochem. Soc. 125 (1978) 228–232.